Monthly Notices
of the
ROYAL ASTRONOMICAL SOCIETY

MNRAS **482,** 1858–1871 (2019)
Advance Access publication 2018 October 16

doi:10.1093/mnras/sty2789

Effects of anisotropic stress in interacting dark matter – dark energy scenarios

Weiqiang Yang [1]★ Supriya Pan [2]★ Lixin Xu [3]★ and David F. Mota [4]★

[1] *Department of Physics, Liaoning Normal University, Dalian 116029, P.R. China*
[2] *Department of Mathematics, Raiganj Surendranath Mahavidyalaya, Sudarshanpur, Raiganj, West Bengal 733134, India*
[3] *Institute of Theoretical Physics, School of Physics, Dalian University of Technology, Dalian 116024, P.R. China*
[4] *Institute of Theoretical Astrophysics, University of Oslo, PO Box 1029 Blindern, N-0315 Oslo, Norway*

Accepted 2018 October 11. Received 2018 October 5; in original form 2018 April 29

ABSTRACT

We study a novel interacting dark energy − dark matter scenario where the anisotropic stress of the large-scale inhomogeneities is considered. The dark energy has a constant equation of state and the interaction model produces stable perturbations. The resulting picture is constrained using different astronomical data aiming to measure the impact of the anisotropic stress on the cosmological parameters. Our analyses show that a non-zero interaction in the dark sector is allowed, while a non-interaction scenario is recovered within 68 per cent CL. The anisotropic stress is also constrained to be small, and its zero value is permitted within 68 per cent CL. The dark energy equation of state, w_x, is also found to be close to '−1' boundary. However, from the ratio of the CMB TT spectra, we see that the model has a mild deviation from the ΛCDM cosmology, while such deviation is almost forbidden from the CMB TT spectra alone. Although the deviation is not much significant, but from this data, we cannot exclude such deviation. Overall, at the background level, the model is close to the ΛCDM cosmology, while at the level of perturbations, a non-zero but a very small interaction in the dark sector is permitted. Perhaps, a more accurate conclusion can be made with the next generation of surveys. We also found that the region, $w_x < -1$, is found to be effective to release the tension on H_0. Finally, from the Bayesian analysis, we find that ΛCDM remains still preferred over the interacting scenarios.

Key words: cosmological parameters – dark energy – dark matter.

1 INTRODUCTION

A remarkable revolution in the dynamical history of the universe has been witnessed in the last several years. Around 20 years back, the distant supernovae of Type Ia (SNIa) first indicated an accelerating expansion of the universe and thereafter a lot of distinct astronomical observations have strengthened such observational prediction. To interpret this acceleration, a hypothetical fluid with negative pressure became necessary and subsequently, cosmological constant was revived into the picture. The cosmological constant, Λ, has a negative equation of state, $P_\Lambda = -\rho_\Lambda$, and together with cold dark matter, the joint scenario ΛCDM has been found to be the best cosmological model, at least according to a series of astronomical measurements. In ΛCDM scenario, both the cosmological constant and the cold dark matter remain conserved separately, as if they are two disjoint sectors. Such model of the universe is widely referred to as the non-interacting cosmological scenario. Unfortunately, the cosmological constant suffers from the fine-tuning problem (also known as the cosmological constant problem), where being time-independent, it reports an unimaginable difference (of the order of 10^{121}) in its value determined in the Planck and low-energy scales. The problem associated with the cosmological constant is not a new detection, it is persisting since long (Weinberg 1989), even before the late-accelerating phase. Thus, attempts have been made aiming to provide with a reasonable justification on the fine-tuning problem (Wetterich 1995). While on the other hand, people have tried to bypass this problem through the introduction of dark energy models (Copeland, Sami & Tsujikawa 2006; Amendola & Tsujikawa 2010; Bamba et al. 2012), we also refer to some specific scalar field dark energy models that may also account for the early scenarios of the universe (de Haro, Amorós & Pan 2016a,b). However, although the introduction of dark energy models relieves the cosmological constant problem, but they raised another serious issue that is widely known as the cosmic coincidence problem (Zlatev, Wang & Steinhardt 1999). Such coincidence problem led to another

★ E-mail: d11102004@163.com (WY); span@research.jdvu.ac.in (SP); lxxu@dlut.edu.cn (LX); mota@astro.uio.no (DFM)

class of cosmological theories that is the theory of non-gravitational interaction between dark matter and dark energy.

The non-gravitational interaction in the dark sector, precisely between dark matter and dark energy is a phenomenological concept that was originally thought to explain the different values of the time-independent cosmological constant (Wetterich 1995), but later on, such concept was found to be very useful to explain the cosmic coincidence problem (Amendola 2000; Chimento et al. 2003; Cai & Wang 2005; Hu & Ling 2006; del Campo, Herrera & Pavón 2008, 2009). Certainly, this led to a large amount of investigations towards this direction where the dark sectors have direct interaction (Billyard & Coley 2000; Barrow & Mota 2003; Barrow & Clifton 2006; Skordis et al. 2006; Koivisto & Mota 2008b; Quartin et al. 2008; Chimento 2010; Valiviita, Maartens & Majerotto 2010; Koivisto, Mota & Zumalacarregui 2012; Thorsrud, Mota & Hervik 2012; Akrami et al. 2013; Faraoni, Dent & Saridakis 2014; Yang & Xu 2014a,b,c; Duniya, Bertacca & Maartens 2015; Pan, Bhattacharya & Chakraborty 2015; Valiviita & Palmgren 2015; Mukherjee & Banerjee 2017; Pan & Sharov 2017; Santos et al. 2017; Sharov et al. 2017; Pan, Mukherjee & Banerjee 2018; also see Pan & Chakraborty 2013; Chen et al. 2014; Pan & Chakraborty 2014; Shahalam et al. 2015, 2017; Cai, Tamanini & Yang 2017; Kumar & Nunes 2017a; Odintsov, Oikonomou & Tretyakov 2017). Such interacting scenarios have good motivation if the particle physics theory is considered because from the particle physics view, mutual interaction between any two fields is a natural phenomenon, irrespective of the nature of the fields. Although the interacting dynamics is complicated and a generalized cosmic scenario, it recovers the non-interaction cosmology as a special case. Thus, the theory of non-gravitational interaction between dark matter and dark energy is a generalized version of the non-interacting dark matter and dark energy cosmologies. Interestingly enough, the observational data at recent time found that the direct interaction between dark matter and dark energy cannot be excluded (Salvatelli et al. 2014; Kumar & Nunes 2016; Nunes, Pan & Saridakis 2016; Yang et al. 2016; Kumar & Nunes 2017b; van de Bruck, Mifsud & Morrice 2017; Yang, Banerjee & Pan 2017a; Yang, Pan & Mota 2017b; Yang, Pan & Barrow 2018). Moreover, very recently, it has been reported that the current tension on the local Hubble constant can be alleviated with the introduction of dark matter and dark energy interactions (Kumar & Nunes 2016; Di Valentino, Melchiorri & Mena 2017). Additionally, the crossing of phantom barrier has also been found to be an easy consequence of the non-gravitational interaction. Thus, the theory of interacting dark energy might be considered to be an appealing field of research and indeed a hot topic for the next generation of the astronomical surveys.

This work presents a general interacting scenario where besides from the non-gravitational interaction between dark matter and dark energy, we also include the possibility of an anisotropic stress. The anisotropic stress appears when the first-order perturbation is considered, and in most of the cases, it is generally neglected. From both theoretical and the observational grounds, the possibility of an anisotropic stress cannot be excluded at all. Although the dimension of the resulting parameters space is increased, but, due to advancements of the astronomical data, the measurement of the anisotropic stress becomes important. The most important thing is to measure the effect of this quantity on the large-scale structure evolution of the concerned cosmological scenario. This is the primary motivation of this work. In particular, looking at the perturbation equations (see Section 2), one can realize that a non-zero value of the anisotropic stress can affect the temperature anisotropy in the cosmic microwave background (CMB) spectra and also on the matter power spectra. Thus, for a detailed understanding of the interacting scenario in its large-scale structure, the anisotropic stress plays a significant role.

Thus, following the above motivation, in a spatially flat Friedmann–Lemaître–Robertson–Walker (FLRW) universe, we study an interacting dark matter–dark energy scenario in the presence of an anisotropic stress and then constrain this model using a series of latest astronomical data from *CMB radiation*, *joint light-curve analysis* (JLA) sample of SNIa, *baryon acoustic oscillations* (BAO) distance measurements, *Hubble parameter measurements* from cosmic chronometers (CC), *weak gravitational lensing (WL)*, and the *local Hubble constant value* from the *Hubble Space Telescope* (*HST*). The analyses are based on the use of publicly available markov chain monte carlo (MCMC) package `cosmomc`, where the convergence of the cosmological parameters follows the well-known Gelman-Rubin statistics.

The work has been organized in the following way. In Section 2, we describe the background and the perturbation equations for the coupled dark energy in presence of the matter-sourced anisotropic stress. Section 3 describes the observational data that we use to analyse the present models. In Section 4, we discuss the constraints on the current model. Finally, Section 5 closes the work with the main findings of this investigation.

2 THE INTERACTING UNIVERSE

In this section we shall describe an interacting cosmological scenario both at background and perturbative levels. To do this, we assume the most general metric for the underlying geometry of the universe which is characterized by the FLRW line element. We also assume that the metric is spatially flat. The evolution equations for a pressureless dark matter and a dark energy fluid in this universe obey the following conservation equations:

$$\rho_c' + 3\mathcal{H}\rho_c = aQ_c = -aQ, \tag{1}$$

$$\rho_x' + 3\mathcal{H}(1+w_x)\rho_x = aQ_x = aQ, \tag{2}$$

where the prime denotes the differentiation with respect to the conformal time τ (i.e. $' \equiv \frac{\mathrm{d}}{\mathrm{d}\tau}$), $\mathcal{H} = a'/a$ is the conformal Hubble parameter, ρ_c, ρ_x are, respectively, the energy densities of cold dark matter and dark energy, and w_x is the barotropic equation of state of the dark energy, which means $w_x = p_x/\rho_x$, here p_x is the pressure of the dark energy fluid and as usual zero pressure is attributed to cold dark matter sector. The quantity $Q\,(=Q_x = -Q_c)$ in the right-hand sides of (1) and (2) is the energy transfer rate between the dark sectors and depending on its sign the direction of energy flow is determined. To be precise, a positive interaction rate ($Q > 0$) assigns the energy flow from dark matter to dark energy, while the negative interaction rate reverses its direction of energy flow. In addition, we consider the presence of non-relativistic baryons (ρ_b) and relativistic radiation (ρ_r) that follow the standard evolution equations, which means they do not take part in the interaction. The dynamics of the spatially flat universe is thus constrained by the Hubble equation:

$$\mathcal{H}^2 = \frac{8\pi G}{3}a^2\rho_\mathrm{tot}, \tag{3}$$

where $\rho_\mathrm{tot} = \rho_c + \rho_x + \rho_\mathrm{b} + \rho_\mathrm{r}$, is the total energy density of the universe. Hence, if the energy transfer rate, Q, is specified, then the evolution equations for ρ_c and ρ_x can fully be determined using the conservation equations (1) and (2) together with the Hubble constraint (3). However, the presence of interaction in the dark sector may significantly affect the large-scale structure of the universe, and hence it becomes necessary to consider the evolution equations for

the interacting model at the perturbative levels. Thus, in order to do so we consider the perturbed FLRW metric (Mukhanov, Feldman & Brandenberger 1992; Ma & Bertschinger 1995; Malik & Wands 2009):

$$\mathrm{d}s^2 = a^2(\tau)\Big[-(1+2\phi)\mathrm{d}\tau^2 + 2\partial_i B\mathrm{d}\tau\mathrm{d}x^i + \Big((1-2\psi)\delta_{ij} + 2\partial_i\partial_j E\Big)\mathrm{d}x^i\mathrm{d}x^j\Big]. \quad (4)$$

Here, the quantities appearing in the above metric (4), namely, ϕ, B, ψ, and E represent the gauge-dependent scalar perturbations. For this perturbed metric (4), using the conservation equations $\nabla_\nu T^{\mu\nu}_A = Q^\mu_A$, where $\sum_{\mathrm{A}} Q^\mu_A = 0$, one can derive the perturbation equations for the dark fluids characterized by the symbol A (for cold dark matter $A = c$, and for dark energy $A = x$). Here, $Q^\mu_A = (Q_A + \delta Q_A)u^\mu + F^\mu_A$, where Q_A presents the transfer rate of the energy flow between the dark fluids and $F^\mu_A = a^{-1}(0, \partial^i f_A)$, is the momentum density transfer relative to the four-velocity vector u^μ in which f_A is the momentum transfer potential. Now, following (Valiviita, Majerotto & Maartens 2008; Majerotto, Valiviita & Maartens 2010) the perturbed energy and momentum balance equations for the interacting dark matter and dark energy scenario, one can write

$$\delta\rho'_A + 3\mathcal{H}(\delta\rho_A + \delta p_A) - 3(\rho_A + p_A)\psi' - k^2(\rho_A + p_A)(v_A + E') = aQ_A\phi + a\delta Q_A, \quad (5)$$

$$\delta p_A + [(\rho_A + p_A)(v_A + B)]' + 4\mathcal{H}(\rho_A + p_A)(v_A + B) + (\rho_A + p_A)\phi - \frac{2}{3}k^2 p_A\pi_A = aQ_A(v + B) + af_A, \quad (6)$$

where prime stands for the differentiation with respect to the conformal time, mentioned earlier, $\mathcal{H}$ is the conformal Hubble rate, and the quantity Π_A is related to the anisotropic stress σ_A of the fluid A. The relation between the peculiar velocity potential v_A and the local volume expansion rate θ_A is $\theta_A = -k^2(v_A + B)$ in the Fourier space with mode k (Kodama & Sasaki 1984; Mukhanov et al. 1992; Ma & Bertschinger 1995; Valiviita et al. 2008; Malik & Wands 2009). Here by $\delta_A = \delta\rho_A/\rho_A$, we mean the density perturbation for the fluid A and momentum transfer potential f_A has been assumed to be the simplest physical choice, which gives its value to zero in the rest frame of dark matter (Valiviita et al. 2008; Koyama, Maartens & Song 2009; Clemson et al. 2012). Hence, the momentum transfer potential takes the expression $k^2 f_A = Q_A(\theta - \theta_c)$, see Yang & Xu (2014a), where $\theta = \theta^\mu_\mu$, is the volume expansion of the total fluid and θ_c is the volume expansion of the cold dark matter fluid.

Now, the pressure perturbation δp_A, for any fluid A, is related as $\delta p_A = c^2_{sA}\delta\rho_A + (c^2_{sA} - c^2_{aA})\rho'_A(v_A + B)$ (Valiviita et al. 2008), which for the dark energy fluid turns out to be $\delta p_x = c^2_{sx}\delta\rho_x + (c^2_{sx} - c^2_{ax})[3\mathcal{H}(1 + w_x)\rho_x - aQ]\theta_x/k^2$.

The evolution of fluid perturbations could be described by the adiabatic speed of sound $c^2_{aA} \equiv p'_A/\rho'_A = w_A - w'_A/[3\mathcal{H}(1 + w_A)]$. In this adiabatic case, the relation between the perturbations of δp_A and $\delta\rho_A$ is related by $\delta p_A = c^2_{aA}\delta\rho_A$. However, for an entropic fluid, the pressure might not be a unique function of the energy density ρ_A. Therefore, there would be another degree of freedom to describe the microproperties of a general fluid. That is the physical speed of sound in the rest frame $c^2_{sA} \equiv (\delta p_A/\delta\rho_A)|_{\mathrm{rf}}$ ('*rf*' represents the rest frame), which is defined in the comoving frame of the fluid. Now, we note that when the entropic perturbation vanishes, the physical sound speed and the adiabatic sound speed vanishes, which means, $c^2_{sA} = c^2_{aA}$. Hence, in the case of entropic fluid such as scalar fields, one needs both its equation of state and its sound speed to have a complete description of dark energy and its perturbations. However, in order to fully describe a dark energy fluid and its perturbations, one should also consider the possibility of an anisotropic stress, even in an isotropic and homogeneous FLRW universe, where the anisotropic stress, $\sigma_A = \frac{2w_A}{3(1+w_A)}\Pi_A$, can be taken as a spatial perturbation.

In the synchronous gauge ($\phi = B = 0$, $\psi = \eta$, and $k^2E = -h/2 - 3\eta$), the evolution equations for density perturbations and velocity perturbations equations for dark energy and dark matter, respectively, read

$$\delta'_x = -(1 + w_x)\left(\theta_x + \frac{h'}{2}\right) - 3\mathcal{H}w'_x\frac{\theta_x}{k^2} - 3\mathcal{H}(c^2_{sx} - w_x)\left[\delta_x + 3\mathcal{H}(1 + w_x)\frac{\theta_x}{k^2}\right] + \frac{aQ}{\rho_x}\left[-\delta_x + \frac{\delta Q}{Q} + 3\mathcal{H}\big(c^2_{sx} - w_x\big)\frac{\theta_x}{k^2}\right], \quad (7)$$

$$\theta'_x = -\mathcal{H}(1 - 3c^2_{sx})\theta_x + \frac{c^2_{sx}}{(1 + w_x)}k^2\delta_x - k^2\sigma_x + \frac{aQ}{\rho_x}\left[\frac{\theta_c - (1 + c^2_{sx})\theta_x}{1 + w_x}\right], \quad (8)$$

$$\delta'_c = -\left(\theta_c + \frac{h'}{2}\right) + \frac{aQ}{\rho_c}\left(\delta_c - \frac{\delta Q}{Q}\right), \quad (9)$$

$$\theta'_c = -\mathcal{H}\theta_c, \quad (10)$$

where the factor $\delta Q/Q$ includes the perturbation term of the Hubble expansion rate δH (Gavela et al. 2010). The effects of anisotropic stress (present in equation 8) can be studied in two distinct ways as follows. The first approach is to assume a parametrized differential equation for σ_x given by Hu (1998):

$$\sigma'_x + 3\mathcal{H}\frac{c^2_{ax}}{w_x}\sigma_x = \frac{8}{3}\frac{c^2_{\mathrm{vis}}}{1 + w_x}\left(\theta_x + \frac{h'}{2} + 3\eta'\right), \quad (11)$$

where c^2_{vis} is the viscous speed of sound that controls the correspondence between the velocity (or metric) shear and the anisotropic stress. In particular, for a relativistic fluid, $c^2_{\mathrm{vis}} = 1/3$, while for a general dark energy fluid, c^2_{vis} is a free parameter and it can be constrained through the observational data (Huey 2004; Koivisto & Mota 2006; Kunz & Sapone 2007; Mota et al. 2007; Koivisto & Mota 2008a; Song et al. 2010; Saltas & Kunz 2011; Amendola et al. 2014; Cardona, Hollenstein & Kunz 2014). Secondly, one may directly assume an appropriate expression for σ_x since the anisotropic stress (external or internal) can be linked to the overdensity of matter (consequently dark matter) or dark energy as shown in Cardona et al. (2014). In this work, we shall follow the second approach, which means, the anisotropic stress linked to the overdensity of dark matter/dark energy. Now, concerning the interacting cosmologies, the presence of externally sourced anisotropic stress or the internally sourced anisotropic stress are equally favoured, and none of the possibilities have been studied so far. So, for the first time, we begin this new analysis with the externally sourced anisotropic stress leaving the second possibility as a future work in this direction. The external anisotropic stress that is linked to the overdensity of dark matter is also known as the matter-sourced anisotropic stress

model having the form

$$\sigma_x = \frac{2}{3}\frac{1}{1+w_x} e_\pi a^n \Delta_m, \tag{12}$$

while when the anisotropic stress is linked to the overdensity of dark energy (similarly, it might be dubbed as the dark-energy-sourced anisotropic stress model)

$$\sigma_x = \frac{2}{3}\frac{1}{1+w_x}\frac{f_\pi}{1+(g_\pi \mathcal{H}/k)^2}\Delta_x, \tag{13}$$

where $\Delta_i = \delta_i - \frac{\rho_i'}{\rho_i}\frac{\theta_i}{k^2}$, is the gauge invariant density perturbations for matter ($i = m$) and dark energy ($i = x$), respectively. The above relations are established on the fact that the anisotropic stress and the overdensity of dark matter (or, dark energy) may modify the gravitational slip in an effective way (Song et al. 2010). The latest analysis on the observational constraints of dark energy with anisotropic stress can be found in Chang & Xu (2014) and Chang, Lu & Xu (2014).

Let us come to the interaction model that we wish to study in this work. Before taking any typical interaction model, we recall that the interaction function Q directly enters into the pressure perturbation for dark energy as (Valiviita et al. 2008)

$$\delta p_x = c_{sx}^2 \delta\rho_x + \left(c_{sx}^2 - c_{ax}^2\right)\left[3\mathcal{H}(1+w_x)\rho_x - aQ\right]\frac{\theta_x}{k^2}. \tag{14}$$

According to the qualitative analysis on the large-scale instability in the dark sector perturbations during the early radiation era (Valiviita et al. 2008), in the pressure perturbation of dark energy (14), the coupling term Q in the pressure perturbation δp_x can lead to a driving term $\frac{aQ}{\rho_x}\left[\frac{\theta_c-(1+c_{sx}^2)\theta_x}{1+w_x}\right]$ that includes the factor $\mathcal{H}\theta_x$, and it becomes very large if w_x is close to '-1'. This causes rapid growth of θ_x. Qualitatively, this is the source of the instability: In the presence of energy–momentum transfer in the perturbed dark fluids, momentum balance requires a runaway growth of the dark energy velocity. In order to avoid the perturbation instability, and based on the phenomenological consideration, we assume the constant equation of state w_x in the interacting dark energy with the energy transfer rate $Q = 3H\xi(1+w_x)\rho_x$. The presence of the factor $(1+w_x)$ in the interaction function does not bother with the dark energy equation of state, and hence the stability of the interaction model in the large-scale structure of the universe rests on the coupling parameter of the interaction. The perturbation equations (7–10) for the specific interaction model turn out to be

$$\begin{aligned}\delta_x' &= -(1+w_x)\left(\theta_x + \frac{h'}{2}\right) \\ &\quad - 3\mathcal{H}\left(c_{sx}^2 - w_x\right)\left[\delta_x + 3\mathcal{H}(1+w_x)\frac{\theta_x}{k^2}\right] \\ &\quad + 3\mathcal{H}\xi(1+w_x)\left[\frac{\theta+h'/2}{3\mathcal{H}} + 3\mathcal{H}(c_{sx}^2 - w_x)\frac{\theta_x}{k^2}\right],\end{aligned}$$

$$\begin{aligned}\theta_x' &= -\mathcal{H}(1-3c_{sx}^2)\theta_x + \frac{c_{sx}^2}{(1+w_x)}k^2\delta_x \\ &\quad - k^2\sigma_x + 3\mathcal{H}\xi\left[\theta_c - (1+c_{sx}^2)\theta_x\right],\end{aligned}$$

$$\delta_c' = -\left(\theta_c + \frac{h'}{2}\right) + 3\mathcal{H}\xi(1+w_x)\frac{\rho_x}{\rho_c}\left(\delta_c - \delta_x - \frac{\theta+h'/2}{3\mathcal{H}}\right),$$

$$\theta_c' = -\mathcal{H}\theta_c,$$

where the matter-sourced anisotropic stress is $\sigma_x = 2/[3(1+w_x)]e_\pi a^n \Delta_m$. In this work, we consider the matter-sourced model with $n = 0$, which means, $\sigma_x = 2/[3(1+w_x)]e_\pi \Delta_m$, as the simplest case in such complicated interacting dynamics. Although there is no such strict restriction to exclude the possibility of anisotropic stress sourced by dark energy, but, however, as the cluster effects of dark energy is smaller compared to the dark matter, the effects of anisotropic stress sourced by dark energy must be weaker with respect to the anisotropic stress sourced by dark matter. As a result, the anisotropic stress sourced by dark matter might be more relevant in this context.

3 OBSERVATIONAL DATA SETS AND THE STATISTICAL TECHNIQUE

In this section, we describe the main observational data that we have used to constrain the cosmological scenarios, and also we outline the statistical methodology. We use various astronomical data ranging from low redshifts to high redshifts, for our analysis. Next, we summarize the data sets with their corresponding references.

(i) *CMB radiation:* The full Planck 2015 low$-l$ temperature-plus-polarization and the high$-l$ $C_l^{TE} + C_l^{EE}$ likelihood ('Planck TT, TE, EE + lowTEB'; Adam et al. 2016; Aghanim et al. 2016) have been used. For the interacting dark energy with matter-sourced anisotropic stress, the amplitude of CMB at low multipole ($l < 30$) is very sensitive to the values due to the fact that the anisotropic stress of dark energy is proportional to the overdensity of dark matter directly. The summation of the Newtonian potential becomes

$$k^2(\Phi+\Psi) = -8\pi G a^2\left(\sum_A \rho_A\Delta_A + \sum_A p_A\Pi_A\right), \tag{15}$$

where Δ_A is the gauge invariant density contrast and Π_A is related to the anisotropic stress σ_A via $\sigma_A = \frac{2}{3}\frac{w_A}{1+w_A}\Pi_A$. Thus, an extra contribution to the integrated Sachs–Wolfe effect due to the existence of anisotropic stress of dark energy is

$$\begin{aligned}-k^2\mathrm{ISW}_{\mathrm{stress}} &= 8\pi G a^2\sum_A p_A\dot{\Pi}_A - 8\pi G a^2\mathcal{H}\Bigg[4\sum_A p_A\Pi_A \\ &\quad + \sum_A(3\rho_A - p_A)\Pi_A - \sum_A\frac{\mathrm{d}\ln w_A}{\mathrm{d}\ln a}p_A\Pi_A\Bigg].\end{aligned} \tag{16}$$

(ii) *JLA:* The JLA sample (Betoule et al. 2014) containing 740 SNIa in the low-redshift range $z \in [0.01, 1.30]$ have been considered.

(iii) *BAO distance measurements:* For BAO data, we mainly use four different data points. In particular, we use the CMASS and LOWZ samples from the latest Data Release 12 of the Baryon Oscillation Spectroscopic Survey, respectively, at the effective redshifts $z_{\mathrm{eff}} = 0.57$ and $z_{\mathrm{eff}} = 0.32$ (Gil-Marín et al. 2016). In addition, we include the 6dF Galaxy Survey measurement at $z_{\mathrm{eff}} = 0.106$ (Beutler et al. 2011), and the Main Galaxy Sample of Data Release 7 of Sloan Digital Sky Survey (SDSS-MGS) at $z_{\mathrm{eff}} = 0.15$ (Ross et al. 2015).

(iv) *Redshift space distortion data:* We employ the redshift space distortion (RSD) measurements from two distinct galaxy samples, the one that includes the CMASS sample with an effective redshift of $z_{\mathrm{eff}} = 0.57$ (Gil-Marín et al. 2017), while the other includes the LOWZ sample with an effective redshift of $z_{\mathrm{eff}} = 0.32$ (Gil-Marín et al. 2017).

(v) *Hubble parameter measurements:* We also employ the recently released CC data with 30 measurements of the Hubble parameter values in the redshift interval $0 < z < 2$ (Moresco et al. 2016). The CC are basically some galaxies that evolve passively and

are the most massive. An accurate measurement of the differential age evolutions dt of such galaxies together with the spectroscopic estimation of dz with high accuracy yields the Hubble parameter value through $H(z) = (1+z)^{-1}\mathrm{d}z/\mathrm{d}t$. For more on the CC, we refer the readers to Moresco et al. (2016).

(vi) *H_0 from the HST*: The present Hubble constant value yielding $H_0 = 73.02 \pm 1.79\,\mathrm{km s^{-1} Mpc^{-1}}$ (Riess et al. 2016) from the *HST* has been used. We label this value as *HST*.

(vii) *WL data:* Finally, we also use the WL data along with the previous data sets. The sample is taken from the Canada–France–Hawaii Telescope Lensing Survey (CFHTLenS) that spans 154 deg^2 in five optical bands. In this survey, 21 sets of cosmic shear correlation functions linked to six redshift bins have been presented, see Refs. Heymans et al. (2013) and Asgari et al. (2017) for details. The tomographic correlation functions measured from the blue galaxy sample and consistent with zero intrinsic alignment nuisance parameter has been named as *blue_sample* and we have used this *blue_sample* for this work. From the likelihood analysis of the CFHTLenS data, one can extract the information of our Universe. Here, the true inverse covariance matrix takes the form $\mathbb{C}^{-1} = \alpha_A \hat{\mathbb{C}}^{-1}$ in which $\alpha_A = (n_\mu - p - 2)/(n_\mu - 1)$, and $\hat{\mathbb{C}}$ is the measured covariance matrix. The inclusion of the anisotropic stress of dark energy certainly modifies the summation of potentials given in equation (15). Moreover, for the presence of anisotropic stress, the lensing potential gains an extra contribution leading to the convergence power spectrum at angular wavenumber l as

$$P_K^{ij}(l) = \int_0^{\eta_H} \mathrm{d}\eta \frac{q_i(\eta) q_j(\eta)}{[f_K(\chi)]^2} \left(1 + \frac{\sum_A p_A \Pi_A}{\sum_A \rho_A \Delta_A}\right)^2 \times P_\delta\left(k = \frac{l}{f_K(\eta)}; \eta\right), \tag{17}$$

where η is the comoving distance, $f_K(\eta)$ is the angular diameter distance out to η and it depends on the curvature scalar K. We note that in this work we have assumed $K = 0$. The quantity η_H is the horizon distance, and $q_i(\eta)$ represents the lensing efficiency function for the redshift bin i, see Heymans et al. (2013) and Asgari et al. (2017) for more discussions.

Now, for the interacting dark energy with matter-sourced anisotropic stress, the amplitude of CMB at low multipole ($l < 30$) is very sensitive to the values of e_π due to the fact that the anisotropic stress of dark energy is proportional directly to the overdensity of dark matter. The summation of the Newtonian potentials becomes

$$\begin{aligned} k^2(\Phi + \Psi) &= -8\pi G a^2 \sum_A \rho_A \Delta_A - 8\pi G a^2 \sum_A p_A \Pi_A \\ &= -8\pi G a^2 (\rho_b \Delta_b + \rho_c \Delta_c + \rho_x \Delta_x + p_x \pi_x) \\ &= -8\pi G a^2 \Big[\rho_b \delta_b + \rho_c \delta_c + \rho_x \delta_x + \Big(3\mathcal{H}(1+w_x)\rho_x \\ &\quad - \frac{1}{2}(5 + 3c_{sx}^2) a Q\Big) \frac{\theta_x}{k^2}\Big], \end{aligned} \tag{18}$$

where π_x is related to the anisotropic stress σ_x through the relation $\sigma_x = \frac{2w_x}{3(1+w_x)}\pi_x$. For the influence of WL, the convergence power spectrum will also be modified by the anisotropic stress in the same way but in the spatial part of the Newtonian potentials.

The likelihood for our analysis is $\mathcal{L} \propto e^{-\chi^2_{\rm tot}/2}$, where $\chi^2_{\rm tot}$ is $\chi^2_{\rm tot} = \chi^2_{\rm JLA} + \chi^2_{\rm BAO} + \chi^2_{\rm RSD} + \chi^2_{\rm CC} + \chi^2_{\rm HST} + \chi^2_{\rm CMB} + \chi^2_{\rm WL}$. We modify the code CAMB (Lewis & Bridle 2002) that is freely available and here we implement a numerical algorithm. This numerical algorithm is called to solve the background equations and after that corresponding to each data set we calculate the $\chi^2_{\rm tot}$ values. Finally, we call another code known as cosmomc, a MCMC package together with a convergence diagnostic (Gelman & Rubin 1992) that is used to extract the cosmological parameters. The parameters space for our present model is $\mathcal{P}_1 \equiv \{\Omega_c h^2, \Omega_b h^2, 100\theta_{\rm MC}, \tau, e_\pi, w_x, \xi, n_s, \log[10^{10} A_s]\}$ (9D space). Here, $\Omega_c h^2$ is the cold dark matter density, $\Omega_b h^2$ is the baryon density, $100\theta_{\rm MC}$ is the ratio of sound horizon to the angular diameter distance, τ is the optical depth, n_s is the scalar spectra index, A_s is the amplitude of the initial power spectrum, and the remaining e_π, w_x, ξ are the model parameters described earlier. Certainly, the inclusion of both the interaction rate (in terms of the coupling strength ξ) and the parameter e_π quantifying the anisotropic stress, extends the parameters space compared to the minimum number of parameters in ΛCDM, see Barrow (2014) for a detailed discussion. Finally, we note that for stable perturbations, one needs to impose $c^2_{sx} \geq 0$. Here, throughout the analysis we have assumed $c^2_{sx} = 1$. In this connection, we mention that since $w_c = 0$ (for CDM), thus, $c^2_{sc} = 0$.

Table 1. The table displays the flat priors on the cosmological parameters used in this work.

Parameter	Prior
$\Omega_c h^2$	[0.01, 0.99]
$\Omega_b h^2$	[0.005, 0.1]
$100\theta_{\rm MC}$	[0.5, 10]
τ	[0.01, 0.8]
n_s	[0.5, 1.5]
$\log[10^{10} A_s]$	[2.4,4]
w_x	[−2, 0]
e_π	[−1, 1]
ξ	[0, 2]

The priors of specific model parameters have been displayed in Table 1.

4 RESULTS AND ANALYSIS

The interacting scenario in presence of the matter-sourced anisotropic stress is the main focus of this work. However, we have also constrained the interacting scenario where no matter-sourced anisotropic stress is present. The motivation of the second analysis is to see how the presence of matter-sourced anisotropic stress affects the cosmological dynamics. In order to constrain both the interacting scenarios, we have used the following observational data:

(i) CMB (Planck TTTEEE+lowTEB),
(ii) CMB+BAO+RSD,
(iii) CMB+BAO+RSD+*HST*,
(iv) CMB+BAO+WL+*HST*,
(v) CMB+BAO+RSD+WL+*HST*+JLA+CC.

For the interacting scenario with matter-sourced anisotropic stress, we have presented the observational summary in Table 2 where the constraints on the model parameters are shown at 68 per cent and 95 per cent confidence level (CL). In Fig. 1, we display the 1D posterior distributions for some selected model parameters for the above observational data. Let us now analyse the observational constraints on the model parameters.

From Table 2, we see that the observational data allow a non-zero interaction between dark matter and dark energy. However, observing the 1σ error bars of the coupling parameter, ξ, one can readily conclude that $\xi = 0$ is allowed by almost all observational

Table 2. 68 per cent and 95 per cent confidence-level constraints on the model parameters of the interacting scenario with anisotropic stress using different combined analyses of the observational data. Here, $\Omega_{m0} = \Omega_{c0} + \Omega_{b0}$.

Parameters	CMB	CMB+BAO + RSD	CMB+BAO+RSD + *HST*	CMB+BAO+WL + *HST*	CMB + BAO + RSD + WL+*HST*+JLA+CC
$\Omega_c h^2$	$0.1202^{+0.0018+0.0062}_{-0.0029-0.0046}$	$0.1164^{+0.0030+0.0048}_{-0.0018-0.0054}$	$0.1195^{+0.0020+0.0043}_{-0.0023-0.0040}$	$0.1232^{+0.0025+0.0094}_{-0.0053-0.0074}$	$0.1201^{+0.0018+0.0053}_{-0.0030-0.0045}$
$\Omega_b h^2$	$0.02227^{+0.00017+0.00032}_{-0.00016-0.00033}$	$0.02233^{+0.00015+0.00031}_{-0.00017-0.00029}$	$0.02229^{+0.00017+0.00029}_{-0.00016-0.00029}$	$0.02227^{+0.00014+0.00029}_{-0.00014-0.00027}$	$0.02228^{+0.00016+0.00027}_{-0.00014-0.00030}$
$100\theta_{MC}$	$1.04048^{+0.00037+0.00071}_{-0.00037-0.00077}$	$1.04074^{+0.00038+0.00071}_{-0.00037-0.00068}$	$1.04052^{+0.00034+0.00063}_{-0.00033-0.00065}$	$1.04031^{+0.00040+0.00086}_{-0.00036-0.00087}$	$1.04052^{+0.00037+0.00072}_{-0.00034-0.00071}$
τ	$0.0656^{+0.0199+0.0399}_{-0.0213-0.0391}$	$0.0707^{+0.0220+0.0380}_{-0.0207-0.0405}$	$0.0648^{+0.0186+0.0347}_{-0.0181-0.0370}$	$0.0731^{+0.0174+0.0347}_{-0.0183-0.0335}$	$0.0653^{+0.0168+0.0326}_{-0.0170-0.0354}$
n_s	$0.9743^{+0.0046+0.0086}_{-0.0045-0.0090}$	$0.9769^{+0.0049+0.0082}_{-0.0045-0.0085}$	$0.9751^{+0.0041+0.0077}_{-0.0041-0.0077}$	$0.9749^{+0.0039+0.0076}_{-0.0038-0.0074}$	$0.9755^{+0.0039+0.0073}_{-0.0039-0.0075}$
$\ln(10^{10}A_s)$	$3.0741^{+0.0397+0.0786}_{-0.0409-0.0788}$	$3.0806^{+0.0439+0.0770}_{-0.0409-0.0809}$	$3.0700^{+0.0396+0.0678}_{-0.0361-0.0726}$	$3.0882^{+0.0340+0.0676}_{-0.0332-0.0659}$	$3.0706^{+0.0356+0.0639}_{-0.0329-0.0674}$
e_π	$0.0852^{+0.0569+0.0812}_{-0.0469-0.0905}$	$0.0586^{+0.0733+0.0981}_{-0.0692-0.0853}$	$0.0361^{+0.0314+0.0802}_{-0.0477-0.0713}$	$-0.0014^{+0.0237+0.0518}_{-0.0248-0.0494}$	$-0.0064^{+0.0194+0.0515}_{-0.0277-0.0423}$
w_x	$-1.0445^{+0.1967+0.3800}_{-0.1373-0.4093}$	$-0.9494^{+0.0392+0.0832}_{-0.0415-0.0838}$	$-1.0349^{+0.0351+0.0842}_{-0.0437-0.0753}$	$-1.1077^{+0.0488+0.0907}_{-0.0455-0.0956}$	$-1.0452^{+0.0408+0.0626}_{-0.0276-0.0755}$
ξ	$0.0895^{+0.0317+0.2348}_{-0.0895-0.0895}$	$0.0931^{+0.0265+0.1311}_{-0.0882-0.0931}$	$0.0829^{+0.0261+0.1017}_{-0.0829-0.0829}$	$0.1343^{+0.0233+0.2251}_{-0.1343-0.1343}$	$0.1119^{+0.0206+0.1831}_{-0.1119-0.1119}$
Ω_{m0}	$0.3088^{+0.0375+0.1015}_{-0.0407-0.1002}$	$0.3160^{+0.0094+0.0169}_{-0.0088-0.0169}$	$0.3036^{+0.0076+0.0153}_{-0.0077-0.0148}$	$0.2962^{+0.0112+0.0265}_{-0.0140-0.0253}$	$0.3021^{+0.0076+0.0144}_{-0.0074-0.0152}$
σ_8	$0.8489^{+0.0346+0.0925}_{-0.0374-0.0932}$	$0.8266^{+0.0132+0.0302}_{-0.0161-0.0281}$	$0.8242^{+0.0145+0.0275}_{-0.0143-0.0293}$	$0.8204^{+0.0318+0.0545}_{-0.0231-0.0608}$	$0.8116^{+0.0188+0.0289}_{-0.0144-0.0335}$
H_0	$68.6361^{+4.0664+12.5331}_{-5.7559-10.9049}$	$66.4256^{+0.9544+1.8935}_{-1.0226-1.7988}$	$68.5197^{+1.0257+1.7763}_{-0.9289-1.9400}$	$70.2674^{+1.0577+2.3953}_{-1.2938-2.2335}$	$68.8154^{+0.7117+1.8013}_{-0.9007-1.6168}$

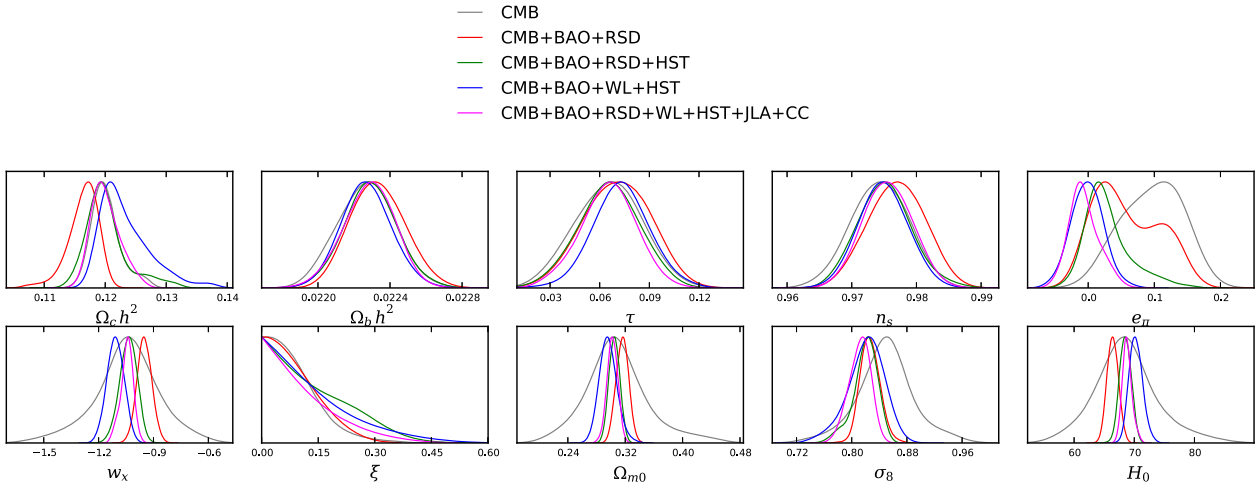

Figure 1. (Color online) The plots show the 1D posterior distributions for various cosmological parameters using different combined analysis of the observational data as displayed in Table 2.

data, which means within 1σ CL, a non-interacting wCDM model is still allowed. From the dark energy equation of state, we find that only CMB and the combined analysis CMB+BAO + RSD hint for its quintessence nature. One can see that the CMB data alone constrain the dark energy equation of state, $w_x = -1.0445^{+0.1967}_{-0.1373}$ at 68 per cent CL ($-1.0445^{+0.3800}_{-0.4093}$ at 95 per cent CL), while from the combination CMB+BAO + RSD, we find $w_x = -0.9494^{+0.0392}_{-0.0415}$ at 68 per cent CL ($-0.9494^{+0.0832}_{-0.0838}$ at 95 per cent CL). One may notice that the addition of BAO and RSD to CMB decreases the error bars in the dark energy equation of state, which means the parameter space for w_x gets reduced. Interestingly enough, when the H_0 prior from the *HST* is included to the other data sets, the dark energy equation of state moves towards the cosmological constant boundary. The combined analysis CMB+BAO+RSD+*HST* shows that $w_x = -1.0349^{+0.0351}_{-0.0437}$ at 68 per cent CL ($-1.0349^{+0.0842}_{-0.0753}$ at 95 per cent CL). The last two analyses, namely, CMB+BAO+WL+*HST* and CMB+BAO+RSD+WL+*HST*+CC+JLA infer the same about the dark energy equation of state, see the last two columns of Table 2. Thus, from the results, one can identify that the dark energy sector resembles with the cosmological constant. Hence, one may conclude that although a non-zero deviation from the ΛCDM cosmology is favoured by the observational data, but effectively such deviation is very minimal and hence the model is close to the ΛCDM model. In Fig. 2, we display the 68 per cent and 95 per cent CL contour plots for the combinations (w_x, H_0), (w_x, Ω_{m0}), and (w_x, ξ) using different combined analyses performed in this work. From the left-hand panel of Fig. 2, we find that for lower values of H_0, the dark energy equation of state, w_x has a shifting nature towards the quintessence regime, while from the middle panel of this figure, we observe that, as w_x increases, which means when it shifts towards the quintessence regime, the density parameter for cold dark matter increases. From the right-hand panel of Fig. 2, we show the dependence of coupling parameter ξ with the dark energy equation of state, w_x, from which making any decisive conclusion between the dependence of ξ with w_x looks very hard, in fact, the parameters w_x and ξ look uncorrelated with each other.

The inclusion of H_0 prior from *HST* also affects other cosmological parameters. For instance, from the constraints on the

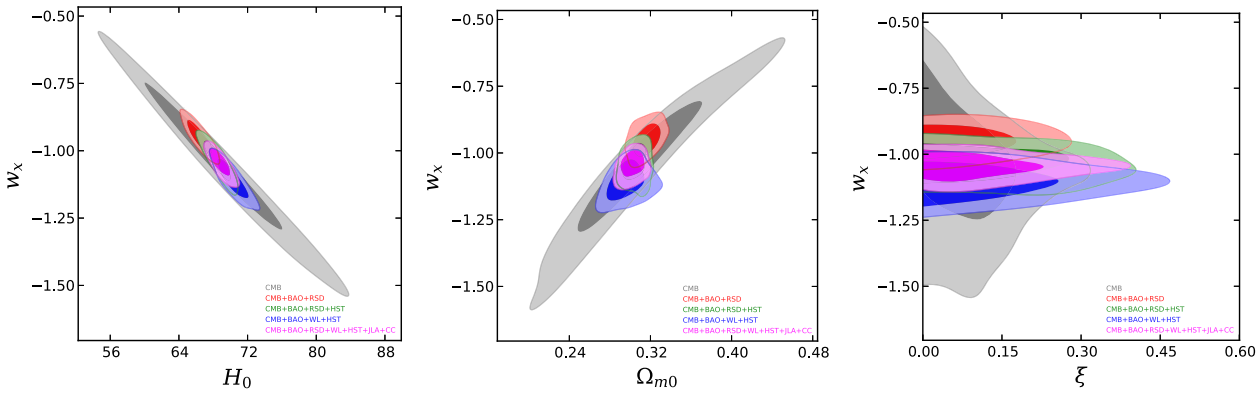

Figure 2. (Color online) 68 per cent and 95 per cent CL contour plots in the 2D (H_0, w_x), (Ω_{m0}, w_x), and (ξ, w_x) planes for different combined analyses have been shown. `Left-hand panel`: This shows that higher values of H_0 allow more phantom nature in the dark energy equation of state w_x, while the quintessence nature is favoured in w_x for lower values of H_0. `Middle Panel`: Higher values of Ω_{m0} favour the quintessence character in the dark energy equation of state, while the phantom character of w_x is increased with the lower values of Ω_{m0}. `Right-hand panel`: The parameters w_x and ξ are almost uncorrelated with each other.

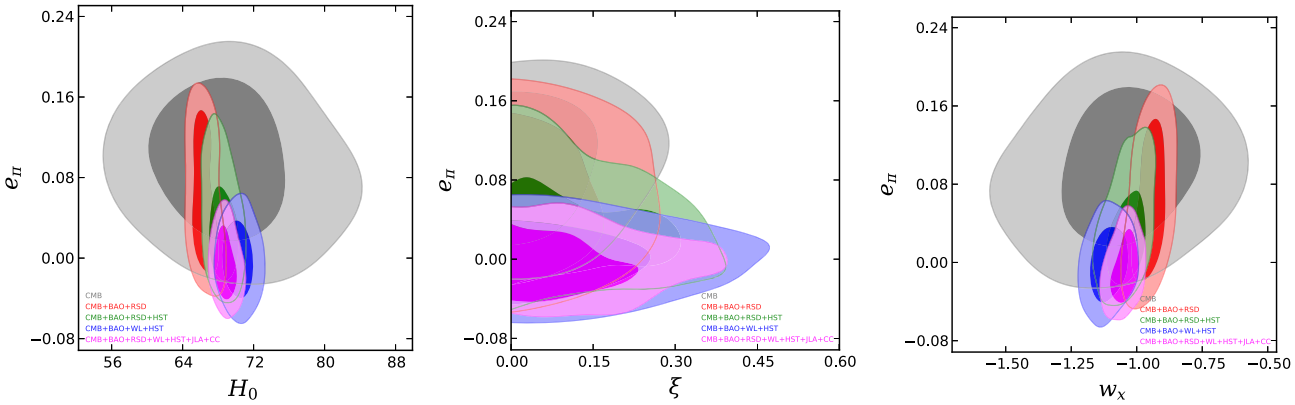

Figure 3. (Color online) 68 per cent and 95 per cent CL contour plots in (e_π, H_0), (e_π, ξ), and (e_π, w_x) planes have been shown for several observational combinations. `Left-hand panel`: This shows the (H_0, e_π) plane. One can see that the combination CMB + ext (where 'ext' is the other data sets, for instance BAO, RSD,.. etc.) decreases the error bars on the parameters. Although, one cannot find a clear relation between e_π and the Hubble parameter values, but the plots for different combinations (except CMB) slightly show that e_π has a very weak tendency to increase its values for lower values of H_0. We repeat that such tendency is extremely weak according to the current data we employ. `Middle Panel`: This actually infers a low-interaction scenario with a small anisotropic stress. However, one can clearly notice that the parameters (e_π, ξ) are almost uncorrelated with each other. `Right-hand panel`: One can see that the phantom dark energy allows lower values of e_π, while for quintessence dark energy one may expect slightly higher values of e_π, although it is clear that the observational data do not allow a large e_π.

anisotropic stress displayed in Table 2 one can find the considerable changes in its constraints. The magnitude of the anisotropic stress significantly changes. The only CMB data constrain $e_\pi = 0.0852^{+0.0569}_{-0.0469}$ at 68 per cent CL ($0.0852^{+0.0812}_{-0.0905}$ at 95 per cent CL), while from CMB+BAO+WL+*HST*, $e_\pi = -0.0014^{+0.0237}_{-0.0248}$ at 68 per cent CL ($-0.0014^{+0.0518}_{-0.0494}$ at 95 per cent CL) and from the full combination CMB+BAO+RSD+WL+*HST*+JLA+CC, it is $e_\pi = -0.0064^{+0.0194}_{-0.0277}$ at 68 per cent CL ($-0.0064^{+0.0515}_{-0.0423}$ at 95 per cent CL). One may observe that there is no such significant change in the error bars in the anisotropic stress. In Fig. 3, we present the 68 per cent and 95 per cent CL contour plots where we show the effects of the anisotropic stress on some selected cosmological parameters, namely, H_0, ξ, and w_x. Additionally, in Fig. 4 we show the σ_8 dependence on other cosmological parameters, namely, e_π, ξ, and H_0.

We now focus on the dynamics of the universe on the large scales for the current cosmological scenario. In Fig. 5, we have plotted the CMB TT power spectra (see the left-hand panel of Fig. 5) and the ratio of the CMB TT power spectra (see the right-hand panel of Fig. 5) for different values of the anisotropic stess e_π and compared the analyses with the base ΛCDM model. It is quite clear from this figure that at low angular scales, for large anisotropic stress, the model deviates vastly from the ΛCDM model, while as the angular scale increases, the deviation reduces from the ΛCDM and at high angular scales, the anisotropic stress does not produce any effective changes in the power spectra. However, the right-hand panel of Fig. 5 says something more that is not visible from the left-hand panel of Fig. 5. From the ratio of CMB TT spectra displayed in the right-hand panel of Fig. 5, one can see that the model still shows a slight deviation from ΛCDM in small angular scales and even if a non-zero value of the anisotropic stress is allowed. Thus, the model has a slight difference from ΛCDM and such a difference is very small. However, we have a very interesting observation from Fig. 6 displaying the CMB TT spectra and the ratio of the CMB TT spectra for different strengths of the coupling parameters. From the left-hand panel of Fig. 6, one can see that a slight deviation of the

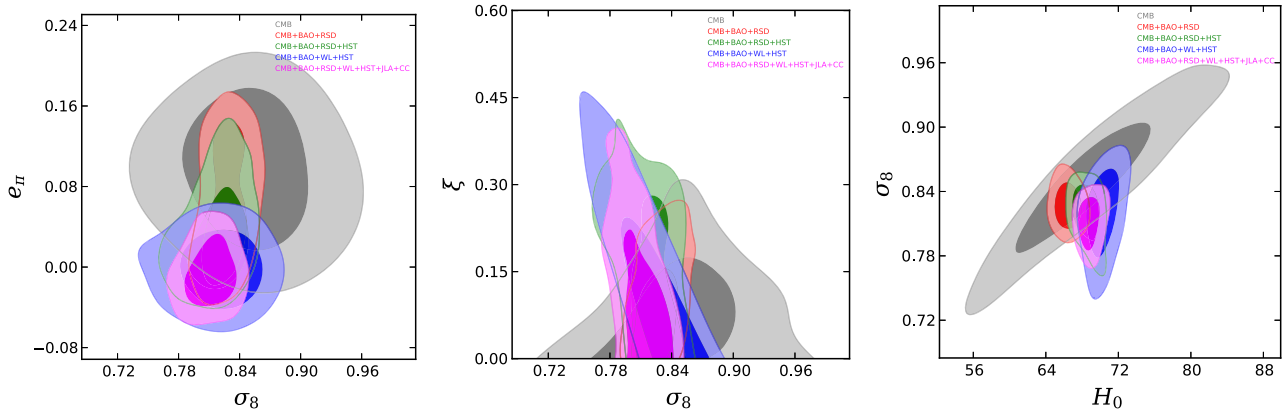

Figure 4. (Color online) 68 per cent and 95 per cent CL contour plots in (σ_8, e_π), (σ_8, ξ), and (H_0, σ_8) planes for several observational combinations. `Left-hand panel`: From the plot, we do not observe any significant effect on σ_8 for anisotropic stress. In fact, one may see that a small value of π is allowed in agreement with the estimated value of σ_8 from Planck Ade et al. (2016). `Middle Panel`: One may notice that σ_8 has a slight dependence on ξ, although such dependence is weak but this is not null. One can see that σ_8 has a tendency to take lower values for increasing strength of the interaction. `Right-hand panel`: A weak dependence between H_0 and σ_8 is reflected from this plot.

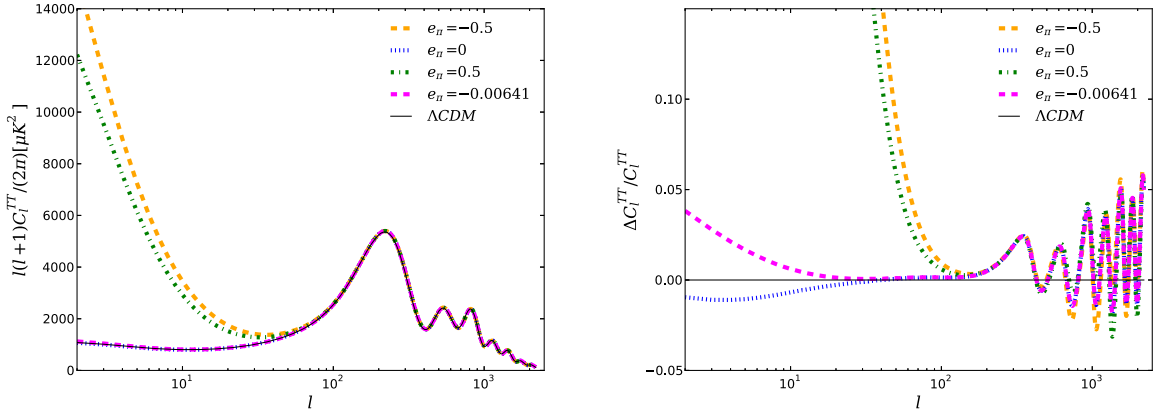

Figure 5. (Color online) The figure shows the CMB TT power spectra (left-hand panel) and the ratio (also known as the relative deviation) of the CMB TT power spectra (right-hand panel) for the present interacting dark-energy scenario $Q = 3H\xi(1 + w_x)\rho_x$ with and without the presence of anisotropic stress that we consider in this work (see Section 2 for details). Here, $\Delta C_l^{\rm TT} = C_l^{\rm TT}\big|_{\rm model} - C_l^{\rm TT}\big|_{\rm LCDM}$ and $C_l^{\rm TT} = C_l^{\rm TT}\big|_{\rm LCDM}$. From the left-hand panel, one may notice that at low angular scales, with the increase of $|e_\pi|$, the deviation from the non-interacting ΛCDM becomes high, but, however, at high angular scales, no such deviation in the CMB TT spectra for $|e_\pi|$ is observed. The similar behaviour is reflected from the right-hand panel, although a non-zero deviation from the ΛCDM even at high angular scales is observed here.

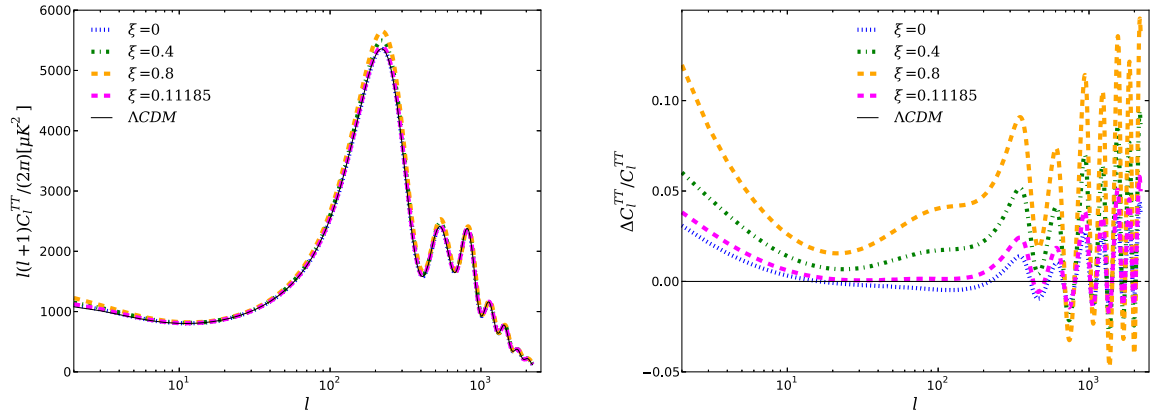

Figure 6. (Color online) The figure shows the CMB TT power spectra (left-hand panel) and the ratio of the CMB TT power spectra (right-hand panel) for the interacting dark-energy scenario in presence of the anisotropic stress considered in this work (described in Section 2). From the left-hand panel, we notice that even in presence of an anisotropic stress sourced by the matter field, the deviation in the CMB TT spectra mainly appears due to large values of the coupling parameter. The right-hand panel confirms the observation of the left-hand panel and additionally a deviation from the ΛCDM.

stressed interacting scenario from the ΛCDM model is observed for a large value of the coupling parameter ($\xi = 0.8$, which is a very big value compared to the observational estimation summarized in Table 2), while from the right-hand panel of Fig. 6, it is quite clear that the model definitely has a deviation from the base ΛCDM for any $\xi \neq 0$. However, the deviation is not much significant.

4.1 Comparison with no-anisotropic stress

In Section 4, we have studied the effects of the anisotropic stress on the cosmological parameters when the dark fluids are interacting with each other. A question that immediately appears in this context is how the contribution of anisotropic stress affects the large-scale structure of the universe and also in the estimation of the cosmological parameters? To answer these questions, we perform similar analyses making $e_\pi = 0$ in the evolution equations with the same priors presented in Table 1. It is quite evident that the analysis with no-anisotropic stress will effectively present a quantitative and qualitative differences on the cosmological parameters. The observational constraints for this particular scenario have been shown in Table 3. The 68 per cent and 95 per cent CL contour plots for some selected parameters have been presented in Fig. 7 where we also show their 1D posterior distributions. From both the analyses, one can clearly notice that except for CMB data only, the exclusion of the anisotropic stress lowers the strength of the coupling parameter. This is an interesting observation in this work that clearly demonstrates that the addition of e_π is the measure of increment in the coupling strength, ξ. However, from the analyses presented in Tables 2 and 3, a clear conclusion that one might draw is, in both the scenarios (with and without anisotropic stress), the coupling strength recovers its zero value within the 68 per cent CL, which means the model w_xCDM+ξ + e_π may recover the non-interacting w_xCDM cosmology within this 68 per cent CL, and this model has a close resemblance with that of the ΛCDM cosmology. This might be considered to be a common behaviour of the models. Furthermore, it should be mentioned that only the combination CMB+BAO+RSD with $e_\pi \neq 0$ does not recover the $\xi = 0$ limit in anyway, and thus, this particular combination always indicates a non-zero interaction in the dark sector.

Probably, the most interesting observation comes from the relative deviation of the CMB TT and matter power spectra shown in Fig. 8. A quick look says that both the scenarios are close to ΛCDM, but there is something more that we would like to describe here. Let us focus on the left-hand panel of Fig. 8 where the relative deviation of the CMB TT spectra has been shown. One can notice that for $l \lesssim 10$, the scenario w_xCDM + ξ + e_π significantly differs from w_xCDM+ξ, and with the increase of l up to a certain value, the difference between the scenarios decreases. We find a particular value of l residing in the region $10 < l < 10^2$ where the difference between the models becomes zero (the point at which both the plots intersect with each other), but, after that, up to some certain l, the difference between the scenarios again increases where the model w_xCDM+ξ + e_π stays far from ΛCDM compared to w_xCDM+ξ. Further, we again notice that the model w_xCDM+ξ + e_π approaches towards ΛCDM and becomes closer compared to the w_xCDM+ξ. And for large l, both the models seem to be indistinguishable from one another. We note that, for all l, the quantity $\Delta C_l^{\rm TT}/C_l^{\rm TT}$ that reports the difference of the model from the ΛCDM is very small.

Now, we concentrate on the relative deviation in the matter power spectra (right-hand panel of Fig. 8), $\Delta P(k)/P(k)$. We remark that for all k, the quantity $\Delta P(k)/P(k)$ is very small informing the closeness of the interacting scenarios towards the ΛCDM model, but, however, we notice some additional features. We find that for very small k, almost for $k \lesssim 10^{-3}$, the quantity $\Delta P(k)/P(k)$ for the model w_xCDM+ξ + e_π is slightly greater compared to the model w_xCDM+ξ, however, for $k \gtrsim 10^{-3}$, the reverse scenario is observed, which means the difference between the interacting scenarios, w_xCDM+ξ + e_π and w_xCDM+ξ, becomes pronounced. Overall, we notice that both the interacting pictures are close to ΛCDM, but indeed, they do not overlap with ΛCDM completely.

Thus, overall, one may conclude that indeed the scenarios w_xCDM+ξ + e_π and w_xCDM+ξ maintain differences amongst each other but for large l (for CMB TT spectra) and large k (matter power spectra), both the scenarios effectively approach toward the Λ-cosmology.

4.2 Easing the tension on H_0?

We now investigate whether the tension on H_0 is released in this context. The tension is one of the most talkative issues at current cosmological research. However, at the very beginning, we recall what exactly the tension on H_0 is. From the estimated values of H_0, one from Planck Ade et al. (2016) (assuming ΛCDM as the base model) and another from Riess et al. (2016) (using the data from *HST*), one can see that the values conflict amongst each other with a sufficient difference between their measurements. From Planck, the estimation of the current Hubble constant is $H_0 = 67.27 \pm 0.66$ km s^{-1} Mpc^{-1}, while the same is reported in Riess et al. (2016) having $H_0 = 73.24 \pm 1.74$ km s^{-1} Mpc^{-1}. Which means the H_0 from Riess et al. (2016) is about 3σ higher from Planck's estimation. This is usually known as the tension on H_0. In the context of interacting dark energy, some latest articles (Kumar & Nunes 2017b; Di Valentino et al. 2017) argued that the allowance of such coupling in the dark sectors becomes efficient to release such tension. Indeed, this is a very potential result because the allowance of extra degrees of freedom in terms of the coupling strength might be able to release such tension. The difference of the earlier works (Kumar & Nunes 2017b; Di Valentino et al. 2017) with the current one is very clear – here we consider the anisotropic stress into the picture, thus, perhaps one may expect slightly different result, and this is the main motivation of this section. Thus, in the first row of Table 4, we have shown the constraints on H_0 for the w_xCDM+ξ + e_π scenario, while the second row of the table shows the constraints on w_xCDM+ξ scenario (i.e. here $e_\pi = 0$, which means no anisotropic stress). One can clearly see that the error bars on H_0 for the CMB analysis are extremely high compared to the other analyses performed. It apparently releases the tension on the H_0 within the 68 per cent CL. On the other hand, from the other analyses, presented in Table 4, one can clearly see that the combination CMB+BAO+WL+*HST* can only relieve the tension on H_0 within 68 per cent CL, while the other combinations do not look promising even at 99 per cent CL. This phenomenon is true for both the interacting scenarios, which means interacting scenario with and without the anisotropic stress.

We investigate this issue more crucially taking the following approach. We consider the interacting scenario w_xCDM+ξ + e_π, for different regions of the dark energy state parameter w_x setting its prior to the following four regions, namely, (i) $w_x \in [-2, -1.2]$, (ii) $w_x \in [-2, -1]$, (iii) $w_x \in [-2, -0.9]$, and finally (iv) $w_x \in [-0.99, -0.9]$. The analyses for the above four choices have been shown in Table 5. One can clearly conclude that as long as the dark energy equation of state remains in the phantom region (i.e. for $w_x \in [-2, -1.2]$), the tension on H_0 can be easily released that fully supports a recent analysis by Di Valentino et al. (2017) finding the

Table 3. 68 per cent and 95 per cent confidendence-level constraints on the model parameters of the interacting scenario with no anisotropic stress for different combined analyses. Here, $\Omega_{m0} = \Omega_{c0} + \Omega_{b0}$.

Parameters	CMB	CMB+BAO + RSD	CMB+BAO+RSD + *HST*	CMB+BAO+WL + *HST*	CMB + BAO + RSD + WL+*HST*+JLA+CC
$\Omega_c h^2$	$0.1214^{+0.0024+0.0052}_{-0.0032-0.0046}$	$0.1180^{+0.0025+0.0042}_{-0.0014-0.0051}$	$0.1206^{+0.0019+0.0085}_{-0.0043-0.0064}$	$0.1190^{+0.0020+0.0044}_{-0.0022-0.0041}$	$0.1183^{+0.0014+0.0030}_{-0.0014-0.0029}$
$\Omega_b h^2$	$0.02220^{+0.00016+0.00029}_{-0.00016-0.00031}$	$0.02223^{+0.00015+0.00030}_{-0.00014-0.00029}$	$0.02229^{+0.00015+0.00029}_{-0.00015-0.00027}$	$0.02226^{+0.00016+0.00027}_{-0.00014-0.00030}$	$0.02231^{+0.00014+0.00029}_{-0.00014-0.00029}$
$100\theta_{MC}$	$1.04038^{+0.00033+0.00064}_{-0.00034-0.00065}$	$1.04055^{+0.00032+0.00066}_{-0.00037-0.00063}$	$1.04058^{+0.00031+0.00063}_{-0.00032-0.00063}$	$1.04040^{+0.00041+0.00069}_{-0.00036-0.00074}$	$1.04065^{+0.00034+0.00060}_{-0.00033-0.00063}$
τ	$0.0778^{+0.0166+0.0326}_{-0.0167-0.0336}$	$0.0674^{+0.0196+0.0371}_{-0.0180-0.0373}$	$0.0704^{+0.0186+0.0368}_{-0.0197-0.0371}$	$0.0748^{+0.0168+0.0359}_{-0.0176-0.0328}$	$0.0663^{+0.0161+0.0315}_{-0.0162-0.0319}$
n_s	$0.9729^{+0.0047+0.0088}_{-0.0044-0.0086}$	$0.9742^{+0.0047+0.0085}_{-0.0039-0.0087}$	$0.9754^{+0.0044+0.0086}_{-0.0045-0.0083}$	$0.9751^{+0.0041+0.0080}_{-0.0043-0.0083}$	$0.9760^{+0.0036+0.0071}_{-0.0038-0.0070}$
$\ln(10^{10}A_s)$	$3.0993^{+0.0330+0.0692}_{-0.0336-0.0675}$	$3.0764^{+0.0382+0.0710}_{-0.0339-0.0725}$	$3.0822^{+0.0369+0.0698}_{-0.0385-0.07034}$	$3.0906^{+0.0330+0.0689}_{-0.0341-0.0636}$	$3.0722^{+0.0311+0.0605}_{-0.0288-0.0616}$
w_x	$-1.0737^{+0.134+0.2517}_{-0.0997-0.3034}$	$-0.9636^{+0.0333+0.1058}_{-0.0595-0.0823}$	$-1.0282^{+0.0406+0.0864}_{-0.0559-0.0802}$	$-1.1040^{+0.0498+0.0909}_{-0.0462-0.0893}$	$-1.0230^{+0.0329+0.0527}_{-0.0257-0.0603}$
ξ	$0.1372^{+0.0382+0.1915}_{-0.1292-0.1372}$	$0.0849^{+0.0222+0.1598}_{-0.0849-0.0849}$	$0.0577^{+0.0170+0.0998}_{-0.0577-0.0577}$	$0.0849^{+0.0209+0.1024}_{-0.0849-0.0849}$	$0.0360^{+0.0091+0.0507}_{-0.0360-0.0360}$
Ω_{m0}	$0.3045^{+0.0279+0.0599}_{-0.0251-0.0646}$	$0.3205^{+0.0086+0.0227}_{-0.0118-0.0187}$	$0.3040^{+0.0083+0.0167}_{-0.0083-0.0163}$	$0.2925^{+0.0088+0.0147}_{-0.0075-0.0163}$	$0.3014^{+0.0070+0.0139}_{-0.0077-0.0141}$
σ_8	$0.8395^{+0.0241+0.0663}_{-0.0308-0.0549}$	$0.8120^{+0.0137+0.0296}_{-0.0146-0.0296}$	$0.8212^{+0.0133+0.0287}_{-0.0166-0.0255}$	$0.8295^{+0.0191+0.0385}_{-0.0179-0.0368}$	$0.8156^{+0.0121+0.0246}_{-0.0137-0.0244}$
H_0	$69.0829^{+2.7931+9.0963}_{-3.9006-6.8847}$	$66.3205^{+1.4094+2.1702}_{-0.9677-2.6570}$	$68.3578^{+1.2570+1.8742}_{-0.9759-2.0948}$	$70.3302^{+1.0053+2.1042}_{-1.1574-1.9285}$	$68.4646^{+0.8199+1.3348}_{-0.7380-1.3616}$

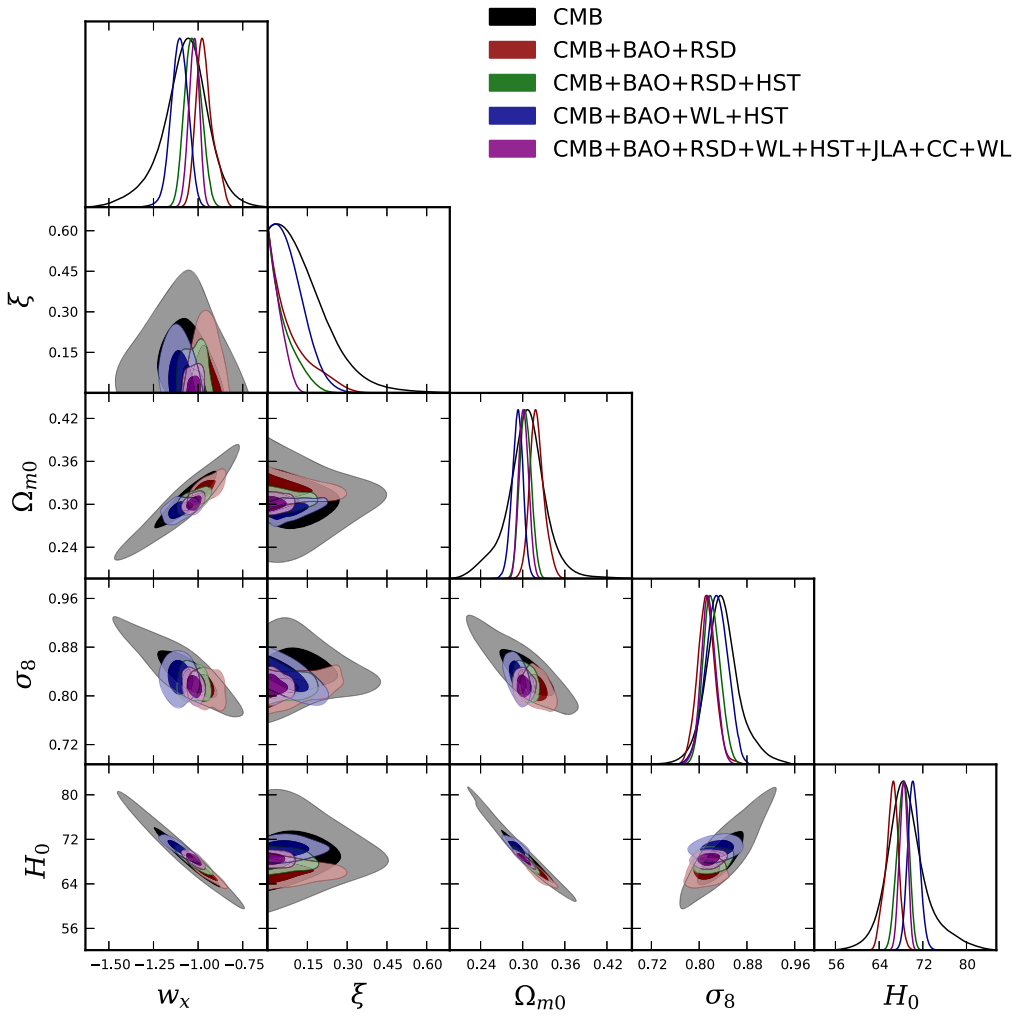

Figure 7. (Color online) 68 per cent and 95 per cent CL contour plots for the interacting scenario with no-anisotropic stress have been shown using different combined analysis. The figure also contains the 2D posterior distributions for the parameters (w_x, ξ, Ω_{m0}, σ_8, H_0). Here, the parameter Ω_{m0} is the current value of $\Omega_m = \Omega_c + \Omega_b$.

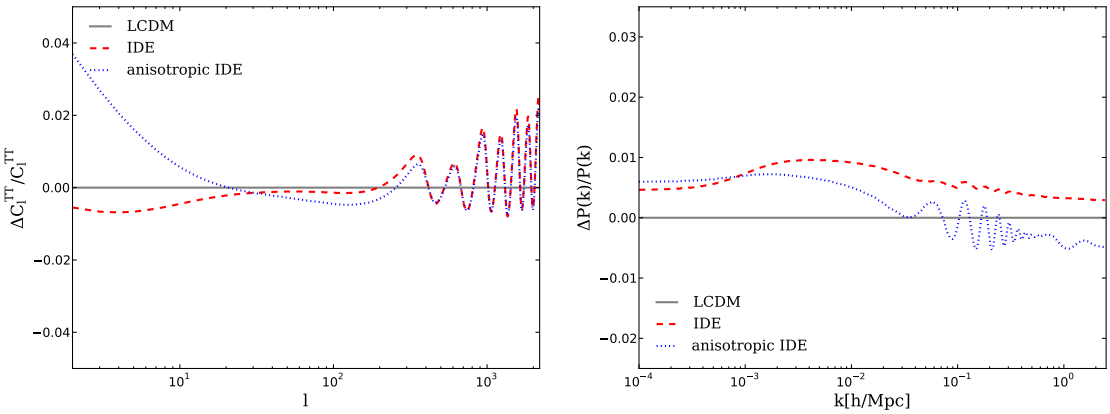

Figure 8. (Color online) The relative deviations in the CMB TT spectra (left-hand panel) and matter power spectra (right-hand panel) have been shown for the interacting scenarios with and without the anisotropic stress using the combined observational data CMB+BAO+RSD+WL+*HST*+JLA+CC.

Table 4. 68 per cent and 95 per cent CL constraints on H_0 for the models with $e_\pi \neq 0$ and $e_\pi = 0$ for different combined analyses of the observtaional data.

Parameters	CMB	CMB+BAO+RSD	CMB+BAO+RSD+*HST*	CMB+BAO+WL+*HST*	CMB + BAO + RSD + WL+*HST*+JLA+CC
H_0 ($e_\pi \neq 0$)	$68.64^{+4.07+12.53+17.61}_{-5.76-10.90-12.82}$	$66.43^{+0.95+1.89+2.44}_{-1.02-1.80-2.38}$	$68.52^{+1.03+1.78+2.73}_{-0.93-1.94-2.51}$	$70.27^{+1.06+2.40+3.25}_{-1.29-2.23-2.67}$	$68.82^{+0.71+1.80+2.46}_{-0.90-1.62-1.95}$
H_0 ($e_\pi = 0$)	$69.08^{+2.79+9.10+12.90}_{-3.90-6.88-10.20}$	$66.32^{+1.41+2.17+2.83}_{-0.97-2.66-2.87}$	$68.36^{+1.26+1.87+2.21}_{-0.98-2.09-2.51}$	$70.33^{+1.01+2.10+2.83}_{-1.16-1.93-2.40}$	$68.46^{+0.82+1.33+1.66}_{-0.74-1.36-1.87}$

Table 5. For different regions of the dark energy state parameter, w_x, we constrain the w_xCDM + ξ + e_π scenario using the combined observational data CMB+BAO+RSD+WL+*HST*+JLA+CC. The table shows the mean values of the cosmological parameters with their errors at 68 per cent and 95 per cent CLs.

Parameters	$w_x \in [-2, -1.2]$	$w_x \in [-2, -1]$	$w_x \in [-2, -0.9]$	$w_x \in [-0.99, -0.9]$
$100\theta_{MC}$	$1.03958^{+0.00039+0.00079}_{-0.00039-0.00078}$	$1.04042^{+0.00035+0.00068}_{-0.00033-0.00068}$	$1.04051^{+0.00041+0.00076}_{-0.00037-0.00084}$	$1.04084^{+0.00032+0.00060}_{-0.00027-0.00062}$
$\Omega_b h^2$	$0.02206^{+0.00013+0.00027}_{-0.00013-0.00026}$	$0.02228^{+0.00014+0.00029}_{-0.00015-0.00029}$	$0.02230^{+0.00015+0.00030}_{-0.00016-0.00030}$	$0.02239^{+0.00014+0.00027}_{-0.00015-0.00027}$
$\Omega_c h^2$	$0.1322^{+0.0049+0.0111}_{-0.0071-0.0109}$	$0.1217^{+0.0024+0.0059}_{-0.0037-0.0052}$	$0.1202^{+0.0024+0.0103}_{-0.0040-0.0064}$	$0.1167^{+0.0012+0.0023}_{-0.0012-0.0023}$
τ	$0.0429^{+0.0162+0.0292}_{-0.0175-0.0317}$	$0.0646^{+0.0162+0.0329}_{-0.0163-0.0345}$	$0.0665^{+0.0184+0.0353}_{-0.0186-0.0362}$	$0.0776^{+0.0168+0.0326}_{-0.0169-0.0345}$
n_s	$0.9681^{+0.0036+0.0075}_{-0.0037-0.0071}$	$0.9746^{+0.0046+0.0078}_{-0.0039-0.0087}$	$0.9763^{+0.0044+0.0086}_{-0.0043-0.0083}$	$0.9790^{+0.0041+0.0076}_{-0.0043-0.0071}$
$\ln(10^{10}A_s)$	$3.0322^{+0.0319+0.0622}_{-0.0335-0.0636}$	$3.0702^{+0.0322+0.0633}_{-0.0323-0.0655}$	$3.0726^{+0.0358+0.0685}_{-0.0362-0.0719}$	$3.0922^{+0.0367+0.0676}_{-0.0328-0.0702}$
e_π	$-0.0361^{+0.0312+0.0531}_{-0.0269-0.0587}$	$-0.0080^{+0.0196+0.0391}_{-0.0192-0.0418}$	$-0.0062^{+0.0202+0.0426}_{-0.0207-0.0392}$	$0.0057^{+0.0179+0.0462}_{-0.0271-0.0410}$
w_x	$-1.2099^{+0.0099+0.0099}_{-0.0018-0.0196}$	$-1.0601^{+0.0431+0.0601}_{-0.0262-0.0654}$	$-1.0391^{+0.0399+0.0862}_{-0.0402-0.1084}$	$-0.9749^{+0.0045+0.0193}_{-0.0150-0.0151}$
ξ	$0.1729^{+0.0948+0.1574}_{-0.1062-0.1729}$	$0.1574^{+0.0416+0.2518}_{-0.1574-0.1574}$	$0.1543^{+0.0740+0.1717}_{-0.1160-0.1543}$	$0.0401^{+0.0103+0.0480}_{-0.0401-0.0401}$
Ω_{m0}	$0.3048^{+0.0133+0.0313}_{-0.0182-0.0298}$	$0.3037^{+0.0077+0.0152}_{-0.0079-0.0147}$	$0.3036^{+0.0070+0.0141}_{-0.0069-0.0138}$	$0.3065^{+0.0059+0.0125}_{-0.0058-0.0122}$
σ_8	$0.7811^{+0.0376+0.0686}_{-0.0355-0.0672}$	$0.8074^{+0.0181+0.0336}_{-0.0182-0.0352}$	$0.8079^{+0.0213+0.0341}_{-0.0140-0.0393}$	$0.8125^{+0.0147+0.0245}_{-0.0128-0.0259}$
H_0	$71.3016^{+0.6542+1.2629}_{-0.6416-1.2947}$	$69.0066^{+0.6404+1.6489}_{-0.9014-1.4568}$	$68.6800^{+0.8318+1.8753}_{-0.8911-1.7090}$	$67.5236^{+0.4626+0.9725}_{-0.4792-1.0026}$

same conclusion. While for the other regions of w_x, we do not find any significant signal for the alleviation of the tension on H_0. We have also shown this result in Fig. 9.

4.3 Bayesian evidence

We close the observational analysis of this work with a comparison of the interacting dark energy scenarios through the Bayesian evidence, an effective approach that enables us to judge the acceptance of the cosmological models compared to some reference model. As usual we adopt the reference model to be the six-parameters based ΛCDM cosmological model. To calculate the Bayesian evidence, we need the posterior probability of the model parameters denoted by Θ, given a specific astronomical data set x for analysing the model, any prior information and the model M. Using the Bayes theorem

$$p(\Theta|x, M) = \frac{p(x|\Theta, M)\,\pi(\Theta|M)}{p(x|M)}, \tag{19}$$

where $p(x|\Theta, M)$ is the likelihood function (this depends on the model parameters Θ with the fixed astronomical data set having $\pi(\Theta|M)$ as the prior information). The quantity $p(x|M)$ located in the denominator of the right-hand side of equation (19) is used for the model comparison and actually, this is the integral over the unnormalized posterior $\tilde{p}(\Theta|x, M) \equiv p(x|\Theta, M)\,\pi(\Theta|M)$ as follows: $E \equiv p(x|M) = \int \mathrm{d}\Theta\, p(x|\Theta, M)\,\pi(\Theta|M)$, which is also cited as the marginal likelihood. Now, let us consider any two models M_i

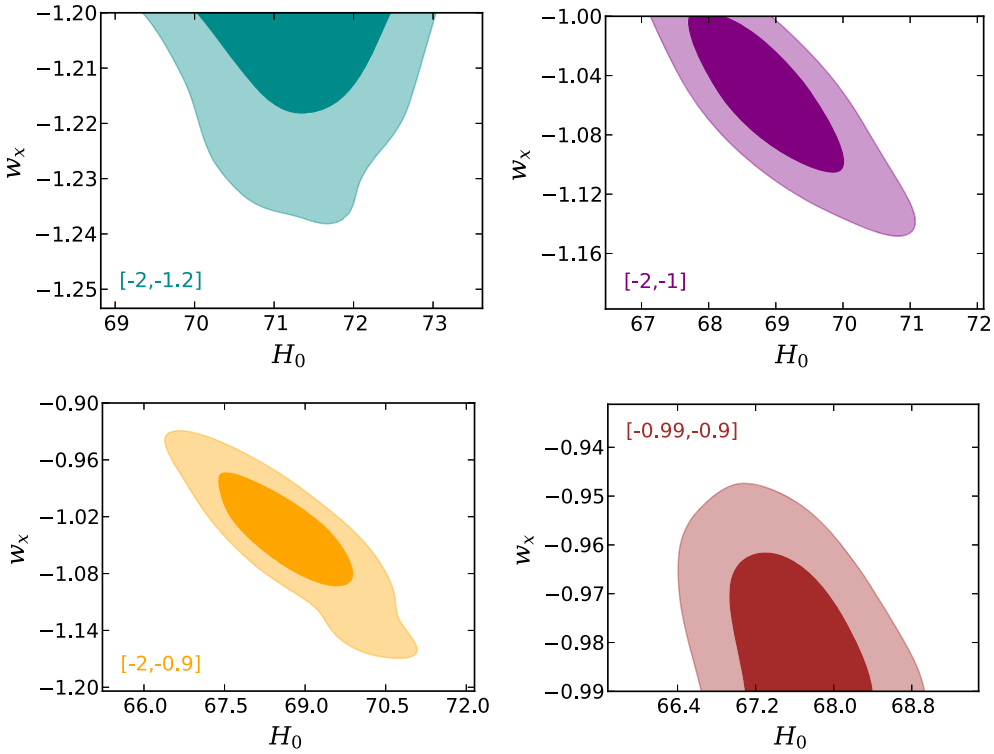

Figure 9. (Color online) 68 per cent and 95 per cent CL contour plots in the fixed plane (H_0, w_x) for different regions of the dark energy state parameter w_x. The combined analysis for this analysis has been fixed to be CMB+BAO+RSD+WL+*HST*+JLA+CC.

Table 6. Revised Jeffreys scale quantifying the observational viability of the model M_i compared to the reference model M_j.

$\ln B_{ij}$	Strength of evidence for model M_i
$0 \leq \ln B_{ij} < 1$	Weak
$1 \leq \ln B_{ij} < 3$	Definite/Positive
$3 \leq \ln B_{ij} < 5$	Strong
$\ln B_{ij} \geq 5$	Very strong

and M_j, where M_i is the model that we want to compare with the reference model M_j (this is the ΛCDM model under consideration). For this case, the posterior probability is given by

$$\frac{p(M_i|x)}{p(M_j|x)} = \frac{\pi(M_i)}{\pi(M_j)}\,\frac{p(x|M_i)}{p(x|M_j)} = \frac{\pi(M_i)}{\pi(M_j)}\,B_{ij}. \tag{20}$$

where $B_{ij} = \frac{p(x|M_i)}{p(x|M_j)}$ is the Bayes factor of the model M_i compared to M_j, the reference model. This factor characterizes the observational viability of the model under consideration as follows: For $B_{ij} > 1$, the astronomical data favour M_i more strongly than M_j. For distinct measures of B_{ij}, sometimes we use $\ln B_{ij}$ for quantification, we follow the Jeffreys scales (Kass & Raftery 1995) summarized in Table 6. The Bayesian evidence is calculated directly from the MCMC chains, the chains used to extract the parameters space of the cosmological models. A detailed description to calculate the Bayesian evidence of any cosmological model can be found at Heavens et al. (2017a,b). We use the publicly available code `MCEvidence`.[1]

[1]Anyone can freely access the code from github.com/yabebalFantaye/MCEvidence.

In Table 7, we summarize the calculated values of $\ln B_{ij}$ for the interacting scenarios (with and without the anisotropic stress) compared to the reference model ΛCDM. The negative values in $\ln B_{ij}$ designate that the ΛCDM model is favoured over the interacting scenarios. We find that for almost all the observational data, the ΛCDM is strongly favoured over both the interacting scenarios (with and without the anisotropic stress).

5 SUMMARY AND CONCLUSIONS

For the first time, we consider an interaction scenario between pressureless dark matter and dark energy when a matter-sourced anisotropic stress is present into the formalism. In general, the contribution from the anisotropic stress is often excluded from the cosmic picture, but, however, a complete cosmological scenario must include all the associated parameters where theoretically, there is no such strong reason to exclude such anisotropic stress. And from the observational point of view, only the analyses might tell us whether the inclusion of anisotropic stress is necessary or not. Thus, keeping the anisotropic stress into our discussions, we try to explore this general interacting scenario. The dark energy equation of state, w_x, in this work has been considered to be time independent, and the interaction rate, Q, has been taken to be of the form $Q = 3H\xi(1 + w_x)\rho_x$ (Yang et al. 2018) in order to investigate the entire parameter space for w_x unlike other interaction models where two separate regions for the dark energy equation of state are considered, see Yang et al. (2018, 2017b) for a detailed motivation behind the choice of the above interaction rate. The cosmological scenario has been constrained for different combinations of the astronomical data with latest compilation (see Table 2).

Our analyses show that the current observational data indicate for a *non-zero interaction in the dark sectors* with a *non-zero*

Table 7. The table summarizes the values of $\ln B_{ij}$ for the interacting scenarios (with and without the anisotropic stress) compared to the reference model ΛCDM model for different data sets. The negative values of $\ln B_{ij}$ according to the Bayesian point of view indicate the preference of ΛCDM model over the interacting scenarios. Here, CBR = CMB+BAO+RSD, CBRH = CMB+BAO+RSD+*HST*, CBWH = CMB+BAO+WL+*HST*, CBRWHJC = CMB+BAO+RSD+WL+*HST*+JLA+CC.

Data set	Model	$\ln B_{ij}$	Strength of evidence for the ΛCDM model
CMB	IDE with anisotropic stress	−3.9	Strong
CBR	IDE with anisotropic stress	−2.2	Definite/Positive
CBRH	IDE with anisotropic stress	−3.8	Strong
CBWH	IDE with anisotropic stress	−5.2	Very strong
CBRWHJC	IDE with anisotropic stress	−4.9	Strong
CMB	IDE with no anisotropic stress	−3.1	Strong
CBR	IDE with no anisotropic stress	−1.9	Definite/Positive
CBRH	IDE with no anisotropic stress	−3.6	Strong
CBWH	IDE with no anisotropic stress	−5.3	Very strong
CBRWHJC	IDE with no anisotropic stress	−4.0	Strong

anisotropic stress in addition. Which means, from the observational base, e_π should not be identically taken to be zero to explore the dynamical features of the universe. Interestingly, most of the combined analyses include $\xi = 0$ and $e_\pi = 0$ within the 68 per cent confidence-region, which means that at the background level the model could mimic the non-interacting w_xCDM model. And moreover, from the estimated values of w_x from different combined analyses, one can also see that w_x is very close to '−1' boundary meaning that the model is actually close to the ΛCDM cosmological model as well. However, the most striking result is observed from the perturbative analysis that reports that *the model is different from the ΛCDM model*. We find that if we allow ξ to be very small (even if we assume $\xi = 0$) but consider the anisotropic stress whatever small its strength be, a deviation from Λ-cosmology is pronounced from the ratio of CMB TT spectra (see the right-hand panel of Fig. 5). On the other hand, even if we make $e_\pi = 0$ and consider different strengths of the interactions (see Fig. 6), then the interaction model shows a deviation from the Λ-cosmology that is only perfectly realized from the ratio of the CMB TT spectra displayed in the right-hand panel of Fig. 6. *This is an interesting result because from the background analysis we could not distinguish* the interaction model from the base ΛCDM, while only the analysis at the perturbative level became able to find out such differences.

We also find that the tension on H_0 can be alleviated. Actually, whenever interaction is present, the release of tension on H_0 is possible as found in some latest investigations (Kumar & Nunes 2016; Di Valentino et al. 2017) where the authors show that the coupling into the dark sector shifts the Hubble parameter value towards its local measurement. Since in this work we consider the anisotropic stress into the picture, hence, we have investigated how the presence of an anisotropic stress controls the tension on H_0. The values of H_0 from different analyses have been shown in Table 4 that clearly shows that the combined analysis CMB+BAO+WL+*HST* could alleviate the tension on the H_0. The analysis with only CMB allows a very large region of H_0 even at 68 per cent CL and thus naturally, the tension is found to be released. While for the other combinations, we do not observe anything similar to that. But, interestingly enough, we find that if we allow w_x to lie within the phantom region only, the tension is surely released (see the second column of Table 5). This result coincides with a latest investigation by Di Valentino et al. (2017), although the major difference with this work is that, here we have an extra degrees of freedom in terms of the anisotropic stress. However, from the Bayesian analysis, we find that the ΛCDM model is well favoured over the present interacting scenarios.

As a closing remark, a number of investigations might be performed following this work. In particular, it is interesting to see the behaviour of the interacting scenario in presence of a dynamical w_x instead of its constant value. The inclusion of massive neutrinos is another important addition in this picture. As the consideration of anisotropic stress is new in the context of coupled dark matter − dark energy models, one can explore some more interesting and important ideas. We hope to address some of them in near future, although such investigations are open to all.

ACKNOWLEDGEMENTS

It is a pleasure to thank the referee of MNRAS for several comments to improve the work. The authors acknowledge the use of publicly available markov chain monte carlo package `cosmomc`. WY acknowledges the support from the National Natural Science Foundation of China under Grants No. 11705079 and No. 11647153. LX acknowledges the support from the National Natural Science Foundation of China under Grants No. 11275035, No.11675032, and 'the Fundamental Research Funds for the Central Universities' under Grant No. DUT16LK31. DFM acknowledges the support from the Research Council of Norway, and this paper is based upon work from COST action CA15117 (CANTATA), supported by COST (European Cooperation in Science and Technology).

REFERENCES

Adam R. et al., 2016, A&A, 594, A1
Ade P. A. R. et al., 2016, A&A, 594, A13
Aghanim N. et al., 2016, A&A, 594, A11
Akrami Y., Koivisto T. S., Mota D. F., Sandstad M., 2013, JCAP, 1310, 046
Amendola L., 2000, Phys. Rev. D, 62, 043511
Amendola L., Tsujikawa S., 2010, Dark Energy. Cambridge Univ. Press, Cambridge
Amendola L., Fogli S., Guarnizo A., Kunz M., Vollmer A., 2014, Phys. Rev. D, 89, 063538
Asgari M., Heymans C., Blake C., Harnois-Deraps J., Schneider P., Van Waerbeke L., 2017, MNRAS, 464, 1676
Bamba K., Capozziello S., Nojiri S., Odintsov S. D., 2012, Ap&SS, 342, 155
Barrow J. D., 2014, Phys. Rev. D, 89, 064022
Barrow J. D., Clifton T., 2006, Phys. Rev. D, 73, 103520
Barrow J. D., Mota D. F., 2003, Class. Quant. Grav., 20, 2045
Betoule M. et al., 2014, A&A, 568, A22
Beutler F. et al., 2011, MNRAS, 416, 3017
Billyard A. P., Coley A. A., 2000, Phys. Rev. D, 61, 083503

Cai R.-G., Wang A., 2005, JCAP, 0503, 002
Cai R.-G., Tamanini N., Yang T., 2017, JCAP, 1705, 031
Cardona W., Hollenstein L., Kunz M., 2014, JCAP, 1407, 032
Chang B., Xu L., 2014, Phys. Rev. D, 90, 027301
Chang B., Lu J., Xu L., 2014, Phys. Rev. D, 90, 103528
Chen X.-m., Gong Y., Saridakis E. N., Gong Y., 2014, Int. J. Theor. Phys., 53, 469
Chimento L. P., 2010, Phys. Rev. D, 81, 043525
Chimento L. P., Jakubi A. S., Pavón D., Zimdahl W., 2003, Phys. Rev. D, 67, 083513
Clemson T., Koyama K., Zhao G.-B., Maartens R., Valiviita J., 2012, Phys. Rev. D, 85, 043007
Copeland E. J., Sami M., Tsujikawa S., 2006, Int. J. Mod. Phys. D, 15, 1753
de Haro J., Amorós J., Pan S., 2016a, Phys. Rev. D, 93, 084018
de Haro J., Amorós J., Pan S., 2016b, Phys. Rev. D, 94, 064060
del Campo S., Herrera R., Pavón D., 2008, Phys. Rev. D, 78, 021302
del Campo S., Herrera R., Pavón D., 2009, JCAP, 0901, 020
Di Valentino E., Melchiorri A., Mena O., 2017, Phys. Rev. D, 96, 043503
Duniya D. G. A., Bertacca D., Maartens R., 2015, Phys. Rev. D, 91, 063530
Faraoni V., Dent J. B., Saridakis E. N., 2014, Phys. Rev. D, 90, 063510
Gavela M. B., Lopez Honorez L., Mena O., Rigolin S., 2010, JCAP, 1011, 044
Gelman A., Rubin D., 1992, Stat. Sci., 7, 457
Gil-Marín H. et al., 2016, MNRAS, 460, 4210
Gil-Marín H., Percival W. J., Verde L., Brownstein J. R., Chuang C.-H., Kitaura F.-S., Rodríguez-Torres S. A., Olmstead M. D., 2017, MNRAS, 465, 1757
Heavens A., Fantaye Y., Mootoovaloo A., Eggers H., Hosenie Z., Kroon S., Sellentin E., 2017a, preprint (arXiv:1704.03472)
Heavens A., Fantaye Y., Sellentin E., Eggers H., Hosenie Z., Kroon S., Mootoovaloo A., 2017b, Phys. Rev. Lett., 119, 101301
Heymans C. et al., 2013, MNRAS, 432, 2433
Hu W., 1998, ApJ, 506, 485
Hu B., Ling Y., 2006, Phys. Rev. D, 73, 123510
Huey G., 2004, preprint (astro-ph/0411102)
Kass R. E., Raftery A. E., 1995, J. Am. Stat. Assoc., 90, 773
Kodama H., Sasaki M., 1984, Prog. Theor. Phys. Suppl., 78, 1
Koivisto T., Mota D. F., 2006, Phys. Rev. D, 73, 083502
Koivisto T., Mota D. F., 2008a, JCAP, 0806, 018
Koivisto T., Mota D. F., 2008b, JCAP, 0808, 021
Koivisto T. S., Mota D. F., Zumalacarregui M., 2012, Phys. Rev. Lett., 109, 241102
Koyama K., Maartens R., Song Y.-S., 2009, JCAP, 0910, 017
Kumar S., Nunes R. C., 2016, Phys. Rev. D, 94, 123511
Kumar S., Nunes R. C., 2017a, Eur. Phys. J. C, 77, 734
Kumar S., Nunes R. C., 2017b, Phys. Rev. D, 96, 103511
Kunz M., Sapone D., 2007, Phys. Rev. Lett., 98, 121301
Lewis A., Bridle S., 2002, Phys. Rev. D, 66, 103511
Majerotto E., Valiviita J., Maartens R., 2010, MNRAS, 402, 2344
Ma C.-P., Bertschinger E., 1995, ApJ, 455, 7
Malik K. A., Wands D., 2009, Phys. Rep., 475, 1
Moresco M. et al., 2016, JCAP, 1605, 014
Mota D. F., Kristiansen J. R., Koivisto T., Groeneboom N. E., 2007, MNRAS, 382, 793
Mukhanov V. F., Feldman H. A., Brandenberger R. H., 1992, Phys. Rep., 215, 203
Mukherjee A., Banerjee N., 2017, Class. Quant. Grav., 34, 035016
Nunes R. C., Pan S., Saridakis E. N., 2016, Phys. Rev. D, 94, 023508
Odintsov S. D., Oikonomou V. K., Tretyakov P. V., 2017, Phys. Rev. D, 96, 044022
Pan S., Chakraborty S., 2013, Eur. Phys. J. C, 73, 2575
Pan S., Chakraborty S., 2014, Int. J. Mod. Phys. D, 23, 1450092
Pan S., Sharov G. S., 2017, MNRAS, 472, 4736
Pan S., Bhattacharya S., Chakraborty S., 2015, MNRAS, 452, 3038
Pan S., Mukherjee A., Banerjee N., 2018, MNRAS, 477, 1189
Quartin M., Calvao M. O., Joras S. E., Reis R. R. R., Waga I., 2008, JCAP, 0805, 007
Riess A. G. et al., 2016, ApJ, 826, 56
Ross A. J., Samushia L., Howlett C., Percival W. J., Burden A., Manera M., 2015, MNRAS, 449, 835
Saltas I. D., Kunz M., 2011, Phys. Rev. D, 83, 064042
Salvatelli V., Said N., Bruni M., Melchiorri A., Wands D., 2014, Phys. Rev. Lett., 113, 181301
Santos L., Zhao W., Ferreira E. G. M., Quintin J., 2017, Phys. Rev. D, 96, 103529
Shahalam M., Pathak S. D., Verma M. M., Khlopov M. Yu., Myrzakulov R., 2015, Eur. Phys. J. C, 75, 395
Shahalam M., Pathak S. D., Li S., Myrzakulov R., Wang A., 2017, Eur. Phys. J. C, 77, 686
Sharov G. S., Bhattacharya S., Pan S., Nunes R. C., Chakraborty S., 2017, MNRAS, 466, 3497
Skordis C., Mota D. F., Ferreira P. G., Boehm C., 2006, Phys. Rev. Lett., 96, 011301
Song Y. S., Hollenstein L., Caldera-Cabral G., Koyama K., 2010, JCAP, 1004, 018
Thorsrud M., Mota D. F., Hervik S., 2012, J. High Energy Phys., 10, 066
Valiviita J., Palmgren E., 2015, JCAP, 1507, 015
Valiviita J., Majerotto E., Maartens R., 2008, JCAP, 0807, 020
Valiviita J., Maartens R., Majerotto E., 2010, MNRAS, 402, 2355
van de Bruck C., Mifsud J., Morrice J., 2017, Phys. Rev. D, 95, 043513
Weinberg S., 1989, Rev. Mod. Phys., 61, 1
Wetterich C., 1995, A&A, 301, 321
Yang W., Xu L., 2014a, Phys. Rev. D, 89, 083517
Yang W., Xu L., 2014b, Phys. Rev. D, 90, 083532
Yang W., Xu L., 2014c, JCAP, 1408, 034
Yang W., Li H., Wu Y., Lu J., 2016, JCAP, 1610, 007
Yang W., Banerjee N., Pan S., 2017a, Phys. Rev. D, 95, 123527
Yang W., Pan S., Mota D. F., 2017b, Phys. Rev. D, 96, 123508
Yang W., Pan S., Barrow J. D., 2018, Phys. Rev. D, 97, 043529
Zlatev I., Wang L.-M., Steinhardt P. J., 1999, Phys. Rev. Lett., 82, 896

This paper has been typeset from a TEX/LATEX file prepared by the author.